Eur. Phys. J. A **31**, 29–42 (2007)
DOI 10.1140/epja/i2006-10165-x

THE EUROPEAN PHYSICAL JOURNAL A

Regular Article – Nuclear Structure and Reactions

Dirac-Brueckner-Hartree-Fock calculations for isospin asymmetric nuclear matter based on improved approximation schemes

E.N.E. van Dalen[a], C. Fuchs, and Amand Faessler

Institut für Theoretische Physik, Universität Tübingen, Auf der Morgenstelle 14, D-72076 Tübingen, Germany

Received: 10 October 2006 / Revised: 15 December 2006
Published online: 25 January 2007 –
Communicated by W. Nazarewicz

Abstract. We present Dirac-Brueckner-Hartree-Fock calculations for isospin asymmetric nuclear matter which are based on improved approximations schemes. The potential matrix elements have been adapted for isospin asymmetric nuclear matter in order to account for the proton-neutron mass splitting in a more consistent way. The proton properties are particularly sensitive to this adaption and its consequences, whereas the neutron properties remains almost unaffected in neutron-rich matter. Although at present full Brueckner calculations are still too complex to apply to finite nuclei, these relativistic Brueckner results can be used as a guidance to construct a density-dependent relativistic mean-field theory, which can be applied to finite nuclei. It is found that an accurate reproduction of the Dirac-Brueckner-Hartree-Fock equation of state requires a renormalization of these coupling functions.

PACS. 21.65.+f Nuclear matter – 21.60.-n Nuclear structure models and methods – 21.30.-x Nuclear forces – 21.30.Fe Forces in hadronic systems and effective interactions

1 Introduction

The investigation of asymmetric matter is of importance for astrophysical and nuclear-structure studies. In the field of astrophysics this investigation is important for the physics of supernova explosions [1] and of neutron stars [2], *e.g.* the chemical composition and cooling mechanism of protoneutron stars [3,4], mass-radius correlations [5,6], and some other topics. In the field of nuclear structure the investigation of isospin asymmetric matter is of interest in study of neutron-rich nuclei [7]. This isovector dependence of the nuclear force can be investigated in heavy-ion experiments [8]. However, the data for neutron-rich nuclei were rather scarce in the past. This situation is changing with the forthcoming new generation of radioactive beam facilities, *e.g.* the future GSI facility FAIR in Germany, the Rare Isotope Accelerator planned in the United States of America or SPIRAL2 at GANIL/France, which will produce large amounts of new data.

Models which make predictions on the nuclear equation of state (EoS) can roughly be divided into three classes: Phenomenological density functionals, effective field theory (EFT) approaches, and *ab initio* approaches. Phenomenological density functionals are based on effective density-dependent interactions such as Gogny or Skyrme forces [9] or relativistic mean-field (RMF) models [10] with usually more than six and less than 15 parameters. The effective field theory approaches lead to a more systematic expansion of the EoS in powers of density, respectively the Fermi momentum k_{F}. The advantage of EFT is the small number of free parameters and a correspondingly higher predictive power. *Ab initio* approaches are based on high-precision free-space nucleon-nucleon interactions and the nuclear many-body problem is treated microscopically. Predictions for the nuclear EoS are essentially parameter free. Examples are variational calculations [11], Brueckner-Hartree-Fock (BHF) [6,12] or relativistic Dirac-Brueckner-Hartree-Fock (DBHF) [13–20] calculations and Green's functions Monte Carlo approaches [21].

Many-body calculations, on the other hand, have to rely on the summation of relevant diagram classes and are still too involved for systematic applications to finite nuclei. However, these results can be used as a guidance for the construction of a "semi"-phenomenological density functional. Examples are, *e.g.*, Gogny forces [22] derived from G-matrices or density-dependent relativistic mean-field (DDRMF) theory [23,24], which can be based on DBHF results.

The theoretical predictions for the isospin dependence of nuclear interactions are still diverse. RMF the-

[a] e-mail: eric.van-dalen@uni-tuebingen.de

ory cannot describe the complex nonlinear behavior of the DBHF and BHF binding energy at densities near $\rho = 0$. Furthermore, the symmetry energy in relativistic DBHF calculations is found to be significantly stiffer than in non-relativistic BHF approaches [25], in particular at high densities. The BHF calculations [26] predict a proton-neutron mass splitting of $m^*_{\mathrm{NR},n} > m^*_{\mathrm{NR},p}$ in neutron-dominated nuclear matter. In contrast, RMF theory with the scalar isovector δ-meson included predict the opposite behavior, $m^*_{\mathrm{D},n} < m^*_{\mathrm{D},p}$ [8,27]. The various Skyrme forces give opposite predictions for the neutron-proton mass splitting. Relativistic *ab initio* calculations based on realistic nucleon-nucleon interactions, as for instance the DBHF approach, are the proper tool to answer these questions.

In this work we describe asymmetric nuclear matter in the framework of the relativistic DBHF approach based on projection techniques using the Bonn potential and their bare NN matrix elements V [28]. Furthermore, the optimal representation scheme for the T-matrix, the subtracted T matrix representation, is applied. This scheme has previously been applied to asymmetric nuclear matter in refs. [18–20]. However, in the present work we go beyond the approach used in [18–20] in the sense that we improve at a couple of approximations. To be more precise, the Bonn potential has now been adapted for asymmetric nuclear matter.

In the solution of the Bethe-Salpeter (BS) equation we abandon the approximation of an averaged np mass in the np channel and distinguish explicitly between the different isospin-dependent matrix elements. As a consequences, the potential and T-matrix are evaluated in terms of six independent helicity or covariant amplitudes instead of five [15], which are sufficient in the case of an averaged np mass.

The plan of this paper is as follows. The relativistic DBHF approach with emphasis on the treatment of the nn, pp, and np channels is treated in sect. 2. Results are presented in sect. 3. Furthermore, the relation between DBHF results and the RMF theory is discussed in sect. 4.2. Finally, we end with a summary and a conclusion in sect. 5.

2 DBHF approach in isospin asymmetric nuclear matter

In this section the relativistic Brueckner approach is discussed. First a general overview is given, followed by a more detailed discussion of the modifications, which are necessary to account properly for the proton-neutron mass splitting and the isospin dependence of the corresponding matrix elements.

In the relativistic DBHF approach a nucleon inside nuclear matter is regarded as a dressed particle as a consequence of its interaction with the surrounding nucleons. This interaction of the nucleons is treated in the ladder approximation of the relativistic BS equation

$$T = V + i \int VQGGT, \tag{1}$$

where T denotes the T-matrix, V the bare nucleon-nucleon, Q the Pauli operator, and G the Green's function of an intermediate off-shell nucleon. This Green's function G which describes the propagation of dressed nucleons in the medium fulfills the Dyson equation

$$G = G_0 + G_0 \Sigma G, \tag{2}$$

where G_0 denotes the free nucleon propagator and Σ the self-energy. In the Hartree-Fock approximation this self-energy is given by

$$\Sigma = -i \int_F (\mathrm{Tr}[GT] - GT). \tag{3}$$

Equations (1)-(3) are strongly coupled. Therefore, this set of equations represents a self-consistency problem and has to be iterated until convergence is reached.

The structure of the self-energy follows from the requirement of translational and rotational invariance, hermiticity, parity conservation, and time reversal invariance. The most general form of the Lorentz structure of the self-energy in the nuclear-matter rest frame is given by

$$\Sigma(k, k_\mathrm{F}) = \Sigma_s(k, k_\mathrm{F}) - \gamma_0 \, \Sigma_o(k, k_\mathrm{F}) + \boldsymbol{\gamma} \cdot \mathbf{k} \, \Sigma_v(k, k_\mathrm{F}), \tag{4}$$

where the Σ_s, Σ_o, and Σ_v components are Lorentz scalar functions which depend on the Lorentz invariants k^2, $k \cdot j$ and j^2, with j_μ the baryon current. Therefore, these Lorentz invariants can be expressed in terms of k_0, $|\mathbf{k}|$ and k_F, where k_F denotes the Fermi momentum. The different components of the self-energy are determined by taking the respective traces [29,30]

$$\begin{aligned} \Sigma_s &= \frac{1}{4} \, \mathrm{tr}[\Sigma], \quad \Sigma_o = \frac{-1}{4} \, \mathrm{tr}[\gamma_0 \, \Sigma], \\ \Sigma_v &= \frac{-1}{4|\mathbf{k}|^2} \, \mathrm{tr}[\boldsymbol{\gamma} \cdot \mathbf{k} \, \Sigma]. \end{aligned} \tag{5}$$

The presence of the medium influences the masses and momenta of the nucleons inside nuclear matter. These effective masses and effective momenta of the nucleons can be written as

$$\begin{aligned} m^*(k, k_\mathrm{F}) &= M + \Re e \Sigma_s(k, k_\mathrm{F}), \\ k^{*\mu} &= k^\mu + \Re e \Sigma^\mu(k, k_\mathrm{F}). \end{aligned} \tag{6}$$

By the introduction of reduced quantities, one has the reduced effective mass

$$\tilde{m}^*(k, k_\mathrm{F}) = m^*(k, k_\mathrm{F}) / (1 + \Sigma_v(k, k_\mathrm{F})). \tag{7}$$

and the reduced kinetic momentum

$$\tilde{k}^*_\mu = k^*_\mu / (1 + \Sigma_v(k, k_\mathrm{F})), \tag{8}$$

Hence, The Dirac equation written in terms of these reduced effective masses and momenta has the form

$$[\gamma_\mu \tilde{k}^{*\mu} - \tilde{m}^*(k, k_\mathrm{F})] u(k, k_\mathrm{F}) = 0. \tag{9}$$

To simplify the self-consistency scheme we will work in the quasi-particle approximation, *i.e.* the imaginary part

of the self-energy $\Im m\Sigma$ will be neglected. In addition, the "reference spectrum approximation" [31] is applied in the iteration procedure, *i.e.* the effective mass of the nucleon is assumed to be entirely density dependent ($|\mathbf{k}| = k_{\rm F}$). However, in general the reduced effective mass is density and momentum dependent. Therefore, this method implies that the self-energy itself is only weakly momentum dependent. At the end of the calculation one has of course to verify the consistency of the assumption $\Sigma(k) \approx \Sigma(|\mathbf{k}| = k_{\rm F})$ with the result of the iteration procedure.

The solution of the Dirac equation in eq. (9) provides the positive-energy in-medium nucleon spinor

$$u_\lambda(k, k_{\rm F}) = \sqrt{\frac{\tilde{E}^*(\mathbf{k}) + \tilde{m}^*_{\rm F}}{2\tilde{m}^*_{\rm F}}} \begin{pmatrix} 1 \\ \frac{2\lambda|\mathbf{k}|}{\tilde{E}^*(\mathbf{k})+\tilde{m}^*_{\rm F}} \end{pmatrix} \chi_\lambda \,, \qquad (10)$$

where $\tilde{E}^*(\mathbf{k}) = \sqrt{\mathbf{k}^2 + \tilde{m}^{*2}_{\rm F}}$ denotes the reduced effective energy and χ_λ a two-component Pauli spinor with $\lambda = \pm\frac{1}{2}$[1]. The normalization of the Dirac spinor is thereby chosen as $\bar{u}_\lambda(k, k_{\rm F})u_\lambda(k, k_{\rm F}) = 1$.

2.1 nn and pp channel

It is convenient to reduce a four-dimensional BS integral equation, eq. (1), to a three-dimensional one to solve the scattering problem of two nucleons in the nuclear medium. Therefore, the two-particle propagator iGG in the BS equation has to be replaced by the effective Thompson propagator. The Thompson propagator implies that the time-like component of the momentum transfer in V and T is set equal to zero. Hence, the Thompson propagator restricts the exchanged energy transfer by $\delta(k^0)$ to zero. In addition, the Thompson propagator projects the intermediate nucleons onto positive-energy states. Thus, in the two-particle center-of-mass (c.m.) frame, which is the natural frame for studying two-particle scattering processes, the Thompson equation can be written as [13,30]

$$T(\mathbf{p}, \mathbf{q}, x)|_{\rm c.m.} = V(\mathbf{p}, \mathbf{q}) + \int \frac{{\rm d}^3\mathbf{k}}{(2\pi)^3} V(\mathbf{p}, \mathbf{k}) \frac{m^{*2}_{\rm F}}{E^{*2}(\mathbf{k})} \frac{Q(\mathbf{k}, x)}{2E^*(\mathbf{q}) - 2E^*(\mathbf{k}) + i\epsilon} T(\mathbf{k}, \mathbf{q}, x), \qquad (11)$$

where $\mathbf{q} = (\mathbf{q}_1 - \mathbf{q}_2)/2$ is the relative three-momentum of the initial state and $\mathbf{k}$ and $\mathbf{p}$ are the relative three-momenta of the intermediate and the final states, respectively.

The Thompson equation (11) can be solved applying standard techniques, which are outlined in detail by Erkelenz [32]. To determine the self-energy only positive-energy states are needed. Therefore, it is more convenient to apply the Dirac nucleon propagator [29],

$$G_{\rm D}(k, k_{\rm F}) = [\gamma_\mu k^{*\mu} + m^*(k, k_{\rm F})] 2\pi i \delta(k^{*2} - m^{*2}(k, k_{\rm F})) \times \Theta(k^{*0})\Theta(k_{\rm F} - |\mathbf{k}|), \qquad (12)$$

instead of the full nucleon propagator. Due to the Θ-functions in eq. (12) only positive-energy nucleons are allowed in the intermediate scattering states. In this way, one avoids the delicate problem of infinities in the theory which generally will occur if one includes contributions from negative-energy nucleons in the Dirac sea [15,29].

In the on-shell case for identical particles only five of the sixteen helicity matrix elements are independent which follows from general symmetries [32]. After a partial-wave projection onto the $|JMLS\rangle$-states the Thomas equation reduces to a set of one-dimensional integral equations over the relative momentum $|\mathbf{k}|$. Furthermore, it decouples into three subsystems of integral equations: the uncoupled spin singlet, the uncoupled spin triplet, and the coupled triplet states (appendix B). To achieve this reduction to the one-dimensional integral equations the Pauli operator Q is replaced by an angle-averaged Pauli operator $\overline{Q}$ [29]. Due to deformation of the Fermi sphere to a Fermi ellipsoid in the two-nucleon c.m. frame, $\overline{Q}$ is evaluated for such a Fermi ellipsoid:

$$\overline{Q} = \begin{cases} 0 & \text{for } |\mathbf{k}| < k_{\rm min} \,, \\ \frac{\gamma E^*(k) - E^*_{\rm F}}{\gamma u |\mathbf{k}|} & \text{for } k_{\rm min} < |\mathbf{k}| < k_{\rm max} \,, \\ 1 & \text{for } k_{\rm max} < |\mathbf{k}|, \end{cases} \qquad (13)$$

with $k_{\rm min} = \sqrt{k^2_{\rm F} - u^2 E^2_{\rm F}}$, $k_{\rm max} = \gamma(uE_{\rm F} + k_{\rm F})$, and $u = |\mathbf{u}|$. The partially decoupled set of the one-dimensional integral equations are solved by the matrix inversions techniques of Haftel and Tabakin [33].

Due to the anti-symmetry of these two-nucleon states the total isospin of the two-nucleon system ($I = 0, 1$) can be restored by the standard selection rule

$$(-1)^{L+S+I} = -1. \qquad (14)$$

The five independent partial-wave amplitudes in the helicity representation are obtained from the five independent on-shell amplitudes in the $|JMLS\rangle$ representation [32]. After the summation over the total angular momentum one has the five on-shell plane-wave helicity matrix elements

$$\langle \mathbf{p}\lambda'_1\lambda'_2|T^I(x)|\mathbf{q}\lambda_1\lambda_2\rangle = \sum_J \left(\frac{2J+1}{4\pi}\right) d^J_{\lambda'\lambda}(\theta) \langle \lambda'_1\lambda'_2|T^{J,I}(\mathbf{p}, \mathbf{q}, x)|\lambda_1\lambda_2\rangle, \qquad (15)$$

where θ is the scattering angle between $\mathbf{q}$ and $\mathbf{p}$ with $|\mathbf{p}| = |\mathbf{q}|$. Furthermore, one has $\lambda = \lambda_1 - \lambda_2$ and $\lambda' = \lambda'_1 - \lambda'_2$. The reduced rotation matrices $d^J_{\lambda'\lambda}(\theta)$ are those defined by Rose [34].

Since we determine the T-matrix elements in the two-particle c.m. frame, a representation with covariant operators and Lorentz invariant amplitudes in Dirac space is the most convenient way to Lorentz-transform the T-matrix from the two-particle c.m. frame into the nuclear matter rest frame [29]. Some freedom in the choice of this representation exists, because pseudoscalar (ps) and pseudovector (pv) components cannot uniquely be disentangled for on-shell scattering. This ambiguity is minimized by separating the leading order, *i.e.* the single-meson exchange,

[1] From now on we omit the tilde in this section because in the following we normally deal with $\tilde{m}^*_{\rm F}, \tilde{k}^{*\mu}$.

from the full T-matrix. Therefore, the contributions stemming from the single-π and -η exchange are given in the complete pv representation. For the remaining part of the T-matrix, the ps representation is chosen.

Taking the single-nucleon momentum $\mathbf{k} = (0, 0, k)$ along the z-axis, then we have for the nn and pp channel contributions for the self-energy components in the ps representation scheme:

$$\Sigma_s^{ij}(\mathbf{k}) = \frac{1}{4}\int_0^{k_{\mathrm{F}j}} \frac{\mathrm{d}^3\mathbf{q}}{(2\pi)^3}\frac{m_j^*}{E_{q,j}^*}\Big[4F_S^{ij} - F_{\tilde{S}}^{ij} - 4F_{\tilde{V}}^{ij} - 12F_{\tilde{T}}^{ij} + 4F_{\tilde{A}}^{ij} - F_{\tilde{P}}^{ij}\Big], \tag{16}$$

$$\Sigma_o^{ij}(\mathbf{k}) = \frac{1}{4}\int_0^{k_{\mathrm{F}j}} \frac{\mathrm{d}^3\mathbf{q}}{(2\pi)^3}\Big[-4F_V^{ij} + F_{\tilde{S}}^{ij} - 2F_{\tilde{V}}^{ij} - 2F_{\tilde{A}}^{ij} - F_{\tilde{P}}^{ij}\Big], \tag{17}$$

and

$$\Sigma_v^{ij}(\mathbf{k}) = \frac{1}{4}\int_0^{k_{\mathrm{F}j}} \frac{\mathrm{d}^3\mathbf{q}}{(2\pi)^3}\frac{\mathbf{q}\cdot\mathbf{k}}{|\mathbf{k}|^2 E_{q,j}^*}\Big[-4F_V^{ij} + F_{\tilde{S}}^{ij} - 2F_{\tilde{V}}^{ij} - 2F_{\tilde{A}}^{ij} - F_{\tilde{P}}^{ij}\Big], \tag{18}$$

where $i = j = n$ or $i = j = p$, respectively. In the complete pv representation the nn and pp channel contributions to the self-energy components are given by

$$\Sigma_s^{ij}(\mathbf{k}) = \frac{1}{4}\int_0^{k_{\mathrm{F}j}} \frac{\mathrm{d}^3\mathbf{q}}{(2\pi)^3}\frac{m_j^*}{E_{q,j}^*}\left[4g_S^{ij} - g_{\tilde{S}}^{ij} + 4g_A^{ij} + \frac{m_j^{*2} + m_i^{*2} - 2k^{*\mu}q_\mu^*}{(m_i^* + m_j^*)^2} g_{\widetilde{PV}}^{ij}\right], \tag{19}$$

$$\Sigma_o^{ij}(\mathbf{k}) = +\frac{1}{4}\int_0^{k_{\mathrm{F}j}} \frac{\mathrm{d}^3\mathbf{q}}{(2\pi)^3}\left[g_{\tilde{S}}^{ij} - 2g_A^{ij} - \frac{2E_{k,i}^*(m_j^{*2} - k^{*\mu}q_\mu^*) - E_{q,j}^*(m_j^{*2} - m_i^{*2})}{E_{q,j}^*(m_i^* + m_j^*)^2} g_{\widetilde{PV}}^{ij}\right], \tag{20}$$

and

$$\Sigma_v^{ij}(\mathbf{k}) = \frac{1}{4}\int_0^{k_{\mathrm{F}j}} \frac{\mathrm{d}^3\mathbf{q}}{(2\pi)^3}\frac{\mathbf{q}\cdot\mathbf{k}}{|\mathbf{k}|^2 E_{q,j}^*}\left[g_{\tilde{S}}^{ij} - 2g_A^{ij} - \frac{2k_z^*(m_j^{*2} - k^{*\mu}q_\mu^*) - q_z(m_j^{*2} - m_i^{*2})}{q_z(m_i^* + m_j^*)^2} g_{\widetilde{PV}}^{ij}\right], \tag{21}$$

where $i = j = n$ or $i = j = p$, respectively.

In short, the complete pv representation is applied for $V_{\pi,\eta}$ and the ps representation is used for the $T_{\mathrm{Sub}} = T - V_{\pi,\eta}$ to get the most favorable representation scheme, the subtracted T-matrix representation scheme.

2.2 np channel

Since in isospin asymmetric nuclear matter one has to deal with two distinct nucleons states in the np channel, this channel is more complicated than the nn and pp channel. Working with two distinct nucleons has consequences for the Thompson equation, the Pauli blocking operator, and the number of independent helicity matrix elements.

First, the Bonn potential [28] has to be made suitable to treat distinct particles in the medium. An important difference is that the neutrons and protons have unequal effective masses. These distinct effective masses have to be accounted for, in particular, in the evaluation of the potential matrix elements. The resulting one-boson exchange (OBE) matrix elements can be found in appendix A.

Second, the two-particle propagator iG_iG_j in the BS equation has to be replaced by the Thompson propagator for the np channel. The effective Thompson propagator for this channel is given by

$$g_{np} = iG_nG_p = \frac{m_n^*}{E_n^*}\frac{m_p^*}{E_p^*}\frac{1}{\sqrt{s^*} - E_n^* - E_p^* + i\epsilon}, \tag{22}$$

where $\sqrt{s^*}$ is the invariant mass.

In contrast to the five independent helicity matrix elements in the on-shell case for identical particles, in the np channel six helicity matrix elements are independent [35]. After the partial-wave projection onto the $|JMLS\rangle$-states, using an average direct-exchange contribution in the potential this time the Thompson equation partially decouples into two subsystems of one-dimensional integral equations: the coupled spin singlet-triplet states and the coupled triplet states (appendix B). To achieve the reduction to the one-dimensional integral equations the Pauli operator Q has to be replaced by an angle-averaged Pauli operator $\overline{Q}$ [29]. However, the Pauli operator Q for the np channel has to be modified compared to the one in the nn and pp channel, since it has to be evaluated for Fermi ellipsoids with different sizes. The result for the angle-averaged Pauli operator for the np channel $\overline{Q}_{np}$ with a neutron excess is

$$\overline{Q}_{np} = \begin{cases} \Theta(\gamma u E_{\mathrm{F}n} - \gamma k_{\mathrm{F}n}) & \text{for } |\mathbf{k}| < k_{\min}, \\ 1/2[\cos(\theta_p) - \cos(\theta_n)]\Theta(\theta_n - \theta_p) & \text{for } k_{\min} < |\mathbf{k}| < k_{\max}, \\ 1 & \text{for } k_{\max} < |\mathbf{k}|, \end{cases} \tag{23}$$

with $k_{\min} = \gamma|uE_{\mathrm{F}n} - k_{\mathrm{F}n}|$, $k_{\max} = \gamma(uE_{\mathrm{F}n} + k_{\mathrm{F}n})$,

$$\theta_p = \begin{cases} \arccos\left(\frac{\gamma E_p^*(k) - E_{\mathrm{F}p}^*}{\gamma|\mathbf{k}||\mathbf{u}|}\right) & \text{for } \left|\frac{\gamma E_p^*(k) - E_{\mathrm{F}p}^*}{\gamma|\mathbf{k}||\mathbf{u}|}\right| \le 1, \\ 0 & \text{otherwise,} \end{cases} \tag{24}$$

and

$$\theta_n = \begin{cases} \arccos\left(\frac{E_{\mathrm{F}n}^* - \gamma E_n^*(k)}{\gamma|\mathbf{k}||\mathbf{u}|}\right) & \text{for } \left|\frac{E_{\mathrm{F}n}^* - \gamma E_n^*(k)}{\gamma|\mathbf{k}||\mathbf{u}|}\right| \le 1, \\ \pi & \text{otherwise.} \end{cases} \tag{25}$$

Due to the additional independent helicity matrix element, we will have a sixth independent covariant in the T-matrix representation [35]. However, the problem is that we need to have a decomposition that reduces to the one

used in the symmetric case. The general Lorentz representation of the nine invariants given in [35] fulfill this requirement. Leaving out the three redundant invariants in our case, the additionally constructed covariant is defined as

$$T_6^{I,\mathrm{dir}}(|\mathbf{p}|,\theta,x) = \frac{1}{2}F_6^I(|\mathbf{p}|,\theta,x)((\gamma_\mu)_2 \cdot Q_1^\mu - (\gamma_\mu)_1 \cdot Q_2^\mu) = \frac{1}{2}F_6^I(|\mathbf{p}|,\theta,x)(\gamma_2 \cdot k + \gamma_1 \cdot k), \quad (26)$$

with $Q_i^\mu = (p_i + q_i')^\mu/2m$ for $i = 1, 2$ and $\mathbf{k} = \mathbf{p}_1 + \mathbf{q}_1' = -(\mathbf{p}_2 + \mathbf{q}_2')$ in the c.m. frame. The same sixth covariant is used in ref. [15], while the exchange sixth amplitude given in ref. [15] does not contribute in the self-energy components. Therefore, one gets an additional term in the *np* channel contribution to the neutron self-energy components

$$\Sigma_{s,6}^{np}(\mathbf{k}) = \frac{1}{4}\int_0^{k_{\mathrm{F}p}} \frac{\mathrm{d}^3\mathbf{q}}{(2\pi)^3}\frac{m_p^*}{E_{q,p}^*}\left[4\frac{k^{*\mu}q_\mu^* - m_p^{*2}}{m_p^*}F_6^{np}\right], \quad (27)$$

$$\Sigma_{o,6}^{np}(\mathbf{k}) = \frac{1}{4}\int_0^{k_{\mathrm{F}p}} \frac{\mathrm{d}^3\mathbf{q}}{(2\pi)^3}\left[4m_p^*\frac{E_{k,n}^* - E_{q,p}^*}{E_{q,p}^*}F_6^{np}\right], \quad (28)$$

and

$$\Sigma_{v,6}^{np}(\mathbf{k}) = \frac{1}{4}\int_0^{k_{\mathrm{F}p}} \frac{\mathrm{d}^3\mathbf{q}}{(2\pi)^3}\frac{\mathbf{q}\cdot\mathbf{k}}{|\mathbf{k}|^2 E_{q,p}^*}\left[-4m_p^*\frac{k - q_z}{q_z}F_6^{np}\right] \quad (29)$$

compared to the *nn* and *pp* channel. For the proton a similar additional term arises, where neutrons and protons are interchanged in eqs. (27)-(29). In symmetric nuclear matter with equal effective masses for neutrons and protons, the coefficient of this sixth independent amplitude vanishes, *i.e.* the familiar representation scheme with the five linearly independent covariants is obtained, as expected.

Finally, the total neutron and proton self-energies including all channels can be written as

$$\Sigma^n = \Sigma^{nn} + \Sigma^{np}; \qquad \Sigma^p = \Sigma^{pp} + \Sigma^{pn}, \quad (30)$$

respectively.

3 Results and discussion

In fig. 1 we present the results for the equation of state for various values of the asymmetry parameter $\beta = (n_n - n_p)/n_B$ in the framework of the DBHF approach with a sixth independent amplitude in the *np* channel using the Bonn-A potential. The applied representation is the optimal representation so far, the subtracted T-matrix representation. The two extreme cases are symmetric nuclear matter ($\beta = 0.0$) and neutron matter ($\beta = 1.0$). The symmetric nuclear-matter results and neutron matter results agree with those of refs. [16,18]. The binding energy curves for intermediate values of β lie between these two extreme curves and are slightly higher than in ref. [18]. In addition to that, the binding energy

$$E(n_B,\beta) = E(n_B) + E_{\mathrm{sym}}(n_B)\beta^2 + \mathcal{O}(\beta^4) \quad (31)$$

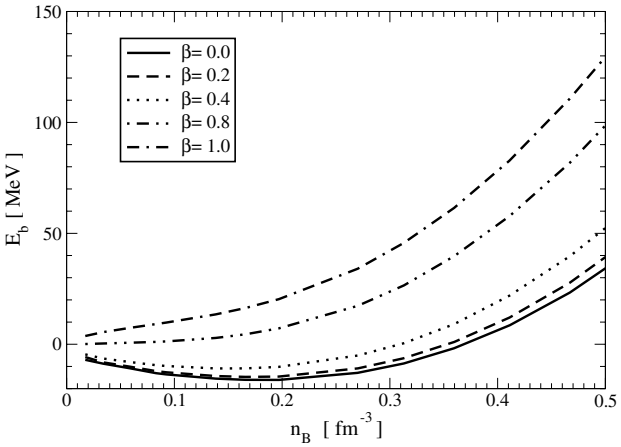

Fig. 1. Binding energy as a function of the baryon density.

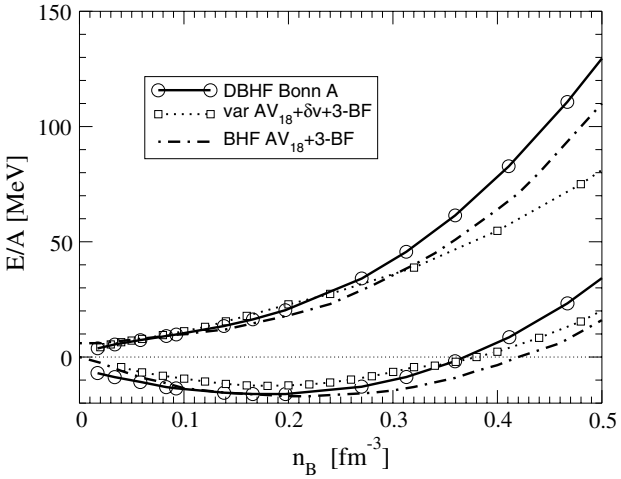

Fig. 2. Comparison of several EoSs from *ab initio* calculations, *i.e.* the present approach (solid line), a nonrelativistic BHF [12] (dash-dotted line) and a variational calculation [11] (dotted line).

shows a nearly quadratic dependence on the asymmetry parameter β as expected.

Figure 2 compares our prediction for the binding energy to the ones of other microscopic many-body approaches, the variational calculations from [11] and the nonrelativistic BHF calculation from [12], at symmetric nuclear matter (below zero) and pure neutron matter (above zero). The variational calculation is based on the high-precision phenomenological Argonne V_{18} [36] two-nucleon interaction and includes UIX three-body forces [37] as well as relativistic boost correction denoted by δv [11]. Also the nonrelativistic BHF calculation [12] is based on the phenomenological Argonne V_{18} [36]. Furthermore, it includes a microscopic three-body force deduced from the meson exchange current approach [12].

The first observation that becomes evident from fig. 2 is that in nuclear matter both, the BHF and DBHF, calculations lead to more binding than the variational calculation. However, in all three cases the EoS of nuclear matter can be characterized as "soft", at least at moderate

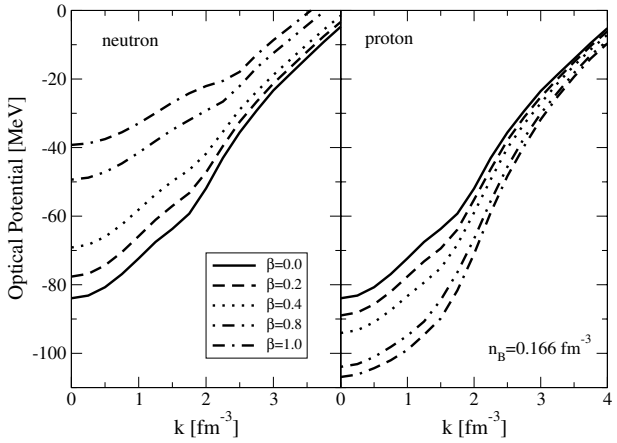

Fig. 3. The neutron and proton optical potential in neutron-rich matter as a function of the momentum $k = |\mathbf{k}|$.

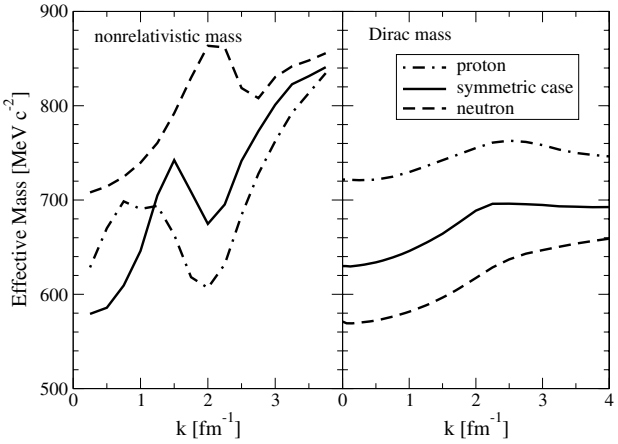

Fig. 4. Neutron and proton effective mass as a function of the momentum $k = |\mathbf{k}|$ in neutron matter at fixed nuclear density $n_B = 0.166\,\mathrm{fm}^{-3}$. In addition, the effective mass in symmetric nuclear matter is given.

densities up to about three times saturation density. The prediction of a soft EoS is the general outcome of a microscopic many-body calculation. Recent quantum Monte Carlo calculations for symmetric nuclear matter [38] show the same tendency. It should be noticed that this observation is supported by corresponding observables extracted from heavy-ion reactions, where supranormal densities up to about three times saturation density are probed. Heavy-ion data for tranverse flow [39] or from kaon production [40] support the picture of a soft EoS in symmetric nuclear matter.

In neutron matter the variational calculations are less stiff, in particular at high-density neutron matter, than our DBHF calculations, whereas the nonrelativistic BHF calculation lies in between these two approaches. However, up to 1.5 times saturation density for neutron matter and symmetric nuclear matter the three approaches show a quite reasonable agreement. This fact indicates that these are the density ranges which are at present reasonable well controlled by state-of-the-art many-body calculations.

The high-density behavior of the EoS, in particular that of the neutron matter EoS, can be constructed by astrophysical observables [4]. The recent observation of the at present heaviest compact star, a binary pulsar of $2.1 \pm 0.2 M_\odot$ (1σ level) [41] rules out very soft neutron matter EoSs. However, all three EoSs shown in fig. 2 fulfill this constraint since they yield maximum neutron star masses between 2.2 and $2.3 M_\odot$.

In fig. 3 the neutron and proton optical potentials are plotted as a function of the momentum $k = |\mathbf{k}|$ for various values of the asymmetry parameter $\beta = (n_n - n_p)/n_B$ at a fixed nuclear density of $n_B = 0.166\,\mathrm{fm}^{-3}$. The depth of the neutron optical potential decreases with increasing asymmetry, whereas the depth of the proton optical potential shows the opposite behavior. Furthermore, the steepness of the neutron optical potential decreases with increasing asymmetry parameter β, whereas the opposite behavior is found in the proton case. Compared to ref. [20] the neutron optical potential remains almost unaltered. In contrast, the proton optical potential lies a bit lower and is somewhat steeper as compared to ref. [20].

The isovector optical potential $U_{\mathrm{iso}} = \frac{U_n - U_p}{2\beta}$ strongly depends on density and momentum. This optical potential in neutron-rich matter initially stays constant and then decreases strongly with increasing momentum. Furthermore, the isovector optical potential is almost independent of the asymmetry parameter β. This behavior can also be observed in refs. [18–20]. Since the proton optical potential lies a bit lower, the isovector optical potential at $k = 0$ is slightly higher than in refs. [18–20]. However, the optical isovector potential at nuclear density $n_B = 0.166\,\mathrm{fm}^{-3}$ at $k = 0$ is still in good agreement with the empirical value of 22–34 MeV [42].

An interesting issue is the proton-neutron mass splitting in neutron-rich matter, which has been discussed in detail in refs. [19,20]. One should keep in mind that different definitions of the effective mass exist, which are often compared and sometimes even mixed up: the nonrelativistic mass and the relativistic Dirac mass. In fig. 4 the nonrelativistic and Dirac effective mass of the neutron and proton are compared for $\beta = 1$, *i.e.* neutron matter. Our DBHF calculations based on projection techniques predict a mass splitting of $m^*_{\mathrm{D},n} < m^*_{\mathrm{D},p}$ in neutron-rich matter. However, the nonrelativistic mass derived from our DBHF approach shows the opposite behavior. This opposite behavior to the relativistic Dirac mass, *i.e.* $m^*_{\mathrm{NR},n} > m^*_{\mathrm{NR},p}$, is in agreement with the results from nonrelativistic BHF calculations [26]. This difference between the Dirac mass splitting and the nonrelativistic mass splitting is not surprising, since these masses are based on completely different physical concepts. The relativistic Dirac mass is defined through the scalar part of the nucleon self-energy in the Dirac field equation which is absorbed into the effective mass (6). On the other hand, the nonrelativistic mass parameterizes the momentum dependence of the single-particle potential.

In this context we want to note that, in contrast to the nonrelativisitc mass m^*_{NR}, the momentum dependence of the Dirac mass m^*_{D} is smooth and still moderate. This fact

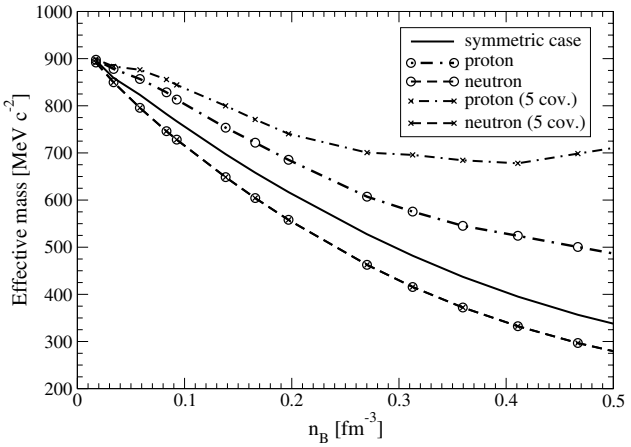

Fig. 5. Neutron and proton effective mass as a function of the density in neutron matter. In addition, the effective mass in symmetric nuclear matter is given. These results are compared to DBHF calculations with average mass assumption in the *np* channel (5 covariants) of refs. [18–20].

is important to justify the reference spectrum approximation, *i.e.* the usage of a momentum-independent effective Dirac mass $\tilde{m}^*_{\rm F}$ for the evaluation of the in-medium spinor basis (10), the Thompson propagator and the potential matrix elements (see appendix A).

In fig. 5 the neutron and proton effective Dirac masses are plotted as a function of the baryon density n_B for pure neutron matter. Of course, a strong density dependence can be observed. In addition, one has a Dirac mass splitting of $m^*_{{\rm D},n} < m^*_{{\rm D},p}$ in the whole density range. RMF field theories with the isovector ρ and δ mesons included predict the same Dirac mass splitting. When only the ρ-meson is included, the RMF theory predicts equal masses. Hence, the δ meson is responsible for the mass splitting in RMF theory.

Furthermore, in fig. 5 our results for the neutron and proton effective Dirac mass in pure neutron matter are compared to those from refs. [18–20], where only 5 covariants were used in the *np* channel. The neutron effective mass remains practically unaffected, whereas the proton mass experiences a sizable reduction. These results are easy to understand. The neutron self-energy consists of a *nn* and a *np* part. Hence, the *nn* part becomes dominant for a vanishing proton fraction. The proton self-energy consists of a *pp* and a *np* part. In the limit of a vanishing proton fraction, the *np* interaction becomes dominant. Therefore, the proton properties, *e.g.* the proton effective mass, are especially sensitive for the treatment of the *np* channel in neutron-rich matter.

4 Relation to relativistic mean-field theory

4.1 DBHF self-energy components

At present full Brueckner calculations are still too complex to allow an application to finite nuclei. However, within the framework of the density-dependent mean-field theory effective density-dependent coupling functions can be obtained from the Brueckner self-energy components. Such coupling functions parameterize the correlations of the T-matrix in a handable way and can be applied to finite nuclei within the framework of DDRMF theory [23]. In contrast to standard RMF models, the meson-baryon vertices are density dependent. As a consequence, rearrangement contributions in the baryon field equations occur. These rearrangement contributions should be taken into account and are essential to satisfy energy momentum conservation and thermodynamic consistency in this density-dependent mean-field theory.

In order to properly parameterize the isospin dependence of the self-energy components, the coupling functions must be based on four different channels: scalar isoscalar, vector isoscalar, scalar isovector, and vector isovector channel. In RMF theory these channels correspond to phenomenological exchange bosons, *i.e.* the σ, ω, δ, and ρ mesons. The effective coupling constants are then given by

$$\left(\frac{g_\sigma(n_B,\beta)}{m_\sigma}\right)^2 = -\frac{1}{2}\frac{\Sigma_{s,p}(k_{{\rm F}p}) + \Sigma_{s,n}(k_{{\rm F}n})}{n_s}\,, \tag{32}$$

$$\left(\frac{g_\omega(n_B,\beta)}{m_\omega}\right)^2 = -\frac{1}{2}\frac{\Sigma_{o,p}(k_{{\rm F}p}) + \Sigma_{o,n}(k_{{\rm F}n})}{n_B}\,, \tag{33}$$

$$\left(\frac{g_\delta(n_B,\beta)}{m_\delta}\right)^2 = -\frac{1}{2}\frac{\Sigma_{s,p}(k_{{\rm F}p}) - \Sigma_{s,n}(k_{{\rm F}n})}{n_{s3}}\,, \tag{34}$$

$$\left(\frac{g_\rho(n_B,\beta)}{m_\rho}\right)^2 = -\frac{1}{2}\frac{\Sigma_{o,p}(k_{{\rm F}p}) - \Sigma_{o,n}(k_{{\rm F}n})}{n_3}\,, \tag{35}$$

with $n_s = n_{sp} + n_{sn}$, $n_B = n_p + n_n$, $n_{s3} = n_{sp} - n_{sn}$, and $n_3 = n_p - n_n$, where

$$n_{si} = \frac{2}{(2\pi)^3}\int_0^{k_{{\rm F}i}} {\rm d}\mathbf{k}\frac{m^*_i}{\sqrt{m^{*2}_i + k^2}} \tag{36}$$

and

$$n_i = \frac{2}{(2\pi)^3}\int_0^{k_{{\rm F}i}} {\rm d}\mathbf{k} = \frac{k^3_{{\rm F}i}}{3\pi^2} \tag{37}$$

are, respectively, the scalar and vector density of the particle $i(= n, p)$. The results for the isoscalar and isovector coupling constants are plotted in figs. 6 and 7, respectively. The strength of the isoscalar coupling functions decreases as the density increases. At low densities, both the scalar g_σ and the vector isoscalar coupling g_ω show a strong decrease with increasing density. However, at higher densities the vector coupling stays more or less constant. The strength in the isovector channel is small compared to that in the isoscalar channel. Furthermore, compared to ref. [18] the dependence on the proton fraction for isovector strength is strongly reduced.

We can directly use these density-dependent coupling functions in a RMF theory for infinite nuclear matter. For practical purposes and to keep the DDRMF functional as simple as possible we ignore in the following the weak isospin dependence and assume only a density dependence in the coupling functions of eqs. (32)-(35). In fig. 8 the

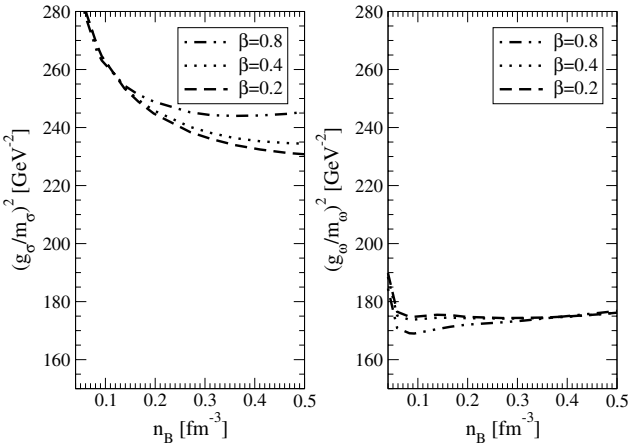

Fig. 6. The isoscalar scalar (g_σ) and vector (g_ω) effective coupling functions are plotted as a function of the baryon density for different values of the asymmetry parameter β.

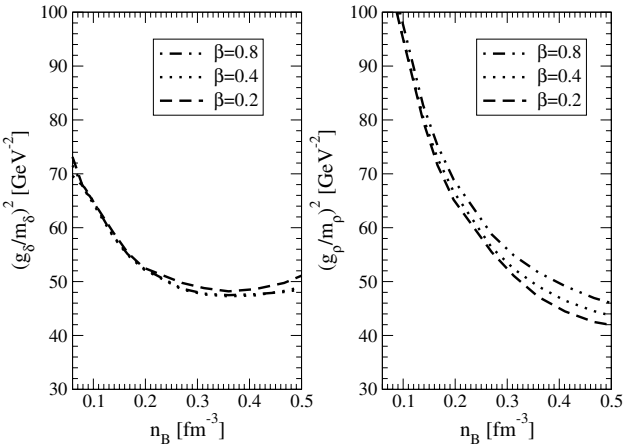

Fig. 7. The isovector scalar (g_δ) and vector (g_ρ) effective coupling functions are plottted as a function of the baryon density for different values of the asymmetry parameter β.

binding energy determined from this RMF theory is compared to our DBHF results for neutron matter and symmetric nuclear matter. The binding energy in RMF theory is given by

$$E/A = \frac{2}{(2\pi)^3}\sum_{i=n,p}\int_{\Theta_{\mathrm{F}i}} \mathrm{d}^3k E_i^*(k) + \frac{1}{2}\left[\left(\frac{g_\sigma(n_B)}{m_\sigma}\right)^2 n_s^2 + \left(\frac{g_\omega(n_B)}{m_\omega}\right)^2 n_B^2 + \left(\frac{g_\delta(n_B)}{m_\delta}\right)^2 n_{s3}^2 + \left(\frac{g_\rho(n_B)}{m_\rho}\right)^2 n_3^2\right], \quad (38)$$

where the density-dependent couplings

$$\left(\frac{g_\alpha(n_B)}{m_\alpha}\right)^2, \quad \alpha \in \{\sigma,\omega,\delta,\rho\} \quad (39)$$

are obtained from eqs. (32)-(35) using the data for $\beta = 0.2$. No rearrangement terms are present in eq. (38), since

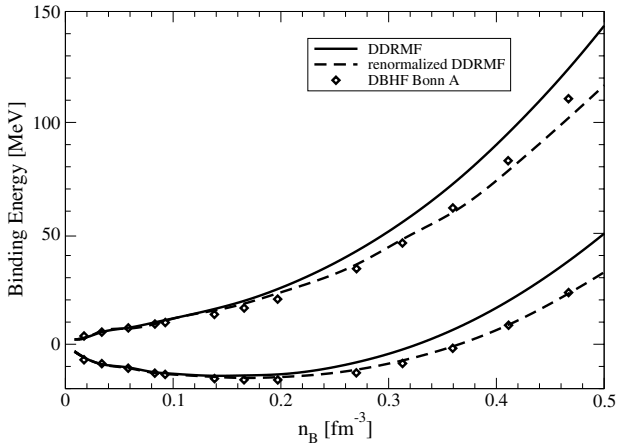

Fig. 8. The DBHF EoS is compared to DDRMF EoS and the renormalized DDRMF EoS.

rearrangement contributions do not contribute at the level of the binding energy [23]. In RMF theory the integral for the kinetic energy can be evaluated and leads to the analytical expression

$$\frac{2}{(2\pi)^3}\sum_{i=n,p}\int_{\Theta_{\mathrm{F}i}} \mathrm{d}^3k E_i^*(k) = \sum_{i=n,p}\left[\frac{3}{4}E_{\mathrm{F}i}n_i + \frac{1}{4}m_i^* n_{s,i}\right] \quad (40)$$

with the Fermi energy $E_{\mathrm{F}i} = \sqrt{k_{\mathrm{F}i}^2 + m_i^{*2}}$. The effective mass contains the contributions of the two scalar mesons. Through the different couplings to the isovector δ-meson this isovector meson accounts for the proton-neutron mass splitting, *i.e.*

$$m_{n/p}^* = M - \left(\frac{g_\sigma(n_B)}{m_\sigma}\right)^2 n_s \pm \left(\frac{g_\delta(n_B)}{m_\delta}\right)^2 n_{s3}\,. \quad (41)$$

Comparing the original DBHF EoS in fig. 8 for the DDRMF EoS based on the parameterization (32)-(35), one observes clear deviations of the two approaches, both for symmetric as well as for neutron matter. This suggests that the density-dependent coupling functions should be extracted more carefully as has been done in the "naive" definition (32)-(35). In other words, an accurate reproduction of the DBHF EoS requires a renormalization of the coupling functions which includes the contributions from Fock terms in a more consistent way.

4.2 Renormalized self-energy components

The fact that renormalization is required when DBHF results are mapped on RMF theory can easily be seen from the DBHF binding energy,

$$E/A = \frac{2}{(2\pi)^3}\sum_{i=n,p}\int_{\Theta_{\mathrm{F}i}} \mathrm{d}^3k\left[E_i^*(k) - \Sigma_{o,i} - \frac{1}{2}\Sigma_{s,i}\frac{m_i^*}{E_i^*} + \frac{1}{2}\frac{\Sigma_{\mu,i}k^{*\mu}}{E_i^*}\right]. \quad (42)$$

The two essential differences between DBHF and RMF concerning the structure of the self-energy, respectively the mean field, are firstly, that the DBHF self-energies carry an explicit momentum dependence and, secondly, the appearance of a nonvanishing spatial contribution Σ_v, see eqs. (4)-(9). Both features should be taken into account as accurate as possible when DBHF results are parameterized in terms of RMF theory. The Σ_v component originates from Fock exchange contributions which are not present in RMF theory. For an accurate reproduction of the DBHF energy functional the spatial Σ_v component has to be included in a proper way. Firstly, the Σ_v component can be absorbed into the effective mass according to eq. (7) and this reduced effective mass has to be identified with RMF effective mass, *i.e.*

$$\tilde{m}_i^* = \frac{M + \Sigma_{s,i}(k_{\mathrm{F}i})}{1 + \Sigma_{v,i}(k_{\mathrm{F}i})} = M + \Sigma_{s,i}^{\mathrm{DDRMF}} \,. \qquad (43)$$

This leads to the renormalized scalar self-energy component

$$\Sigma_{s,i}^{\mathrm{DDRMF}} = \frac{\Sigma_{s,i}(k_{\mathrm{F}i}) - M\Sigma_{v,i}(k_{\mathrm{F}i})}{1 + \Sigma_{v,i}(k_{\mathrm{F}i})} \,. \qquad (44)$$

However, the DBHF energy functional of eq. (42) has additional terms compared to the DDRMF energy functional of eq. (38). In the same way, however, then using the energy density instead of the effective mass, the following expression for the normalized vector self-energy component is obtained:

$$\Sigma_{o,i}^{\mathrm{DDRMF}} = \Sigma_{o,i}(k_{\mathrm{F}i}) - \frac{\Sigma_{v,i}(k_{\mathrm{F}i})[3E_{\mathrm{F}i}n_i + \tilde{m}_i^* n_{s,i}]}{4n_i} \,. \qquad (45)$$

These renormalized self-energy components are now inserted into eqs. (32)-(35) to obtain the renormalized density-dependent coupling functions. By this procedure all terms which contribute to the DBHF energy functional are taken into account in the correspondingly constructed DDRMF functional. However, the explicit momentum dependence in eq. (42) cannot so easily be transferred to the RMF theory which leads still to slight deviation of the corresponding energy functionals. A possibility would be to perform a Taylor expansion of the self-energy components in terms of the momentum [24]. Since the intrinsic momentum dependence of the DBHF self-energy components is generally weak [16,18] we neglect such additional correction terms. The new renormalized isoscalar density-dependent coupling functions are reduced by an amount of 15–20 MeV compared to the corresponding nonrenormalized coupling functions in fig. 6, but the qualitative behavior is very similar. The small isospin dependence of the isoscalar strength is almost insensitive to the renormalization. The renormalized isovector ρ- and δ-meson coupling functions are shown in fig. 9. The density dependence of the renormalized isovector coupling functions is similar to those of fig. 7. However, the β-dependence is now more pronounced.

These renormalized density coupling functions are applied in RMF theory. Again the weak isospin dependence of these coupling functions is ignored. Therefore, we use

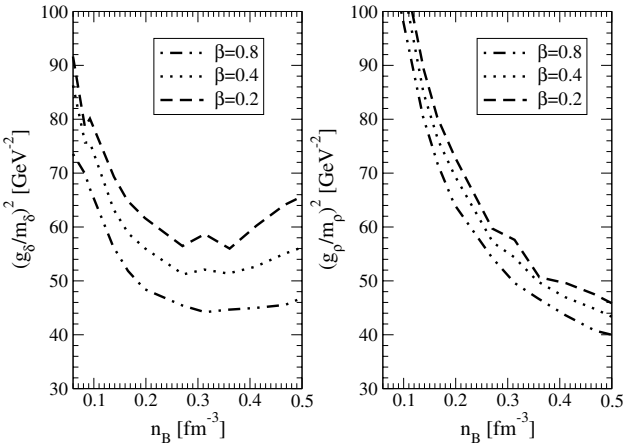

Fig. 9. The renormalized isovector scalar (g_δ) and vector (g_ρ) effective coupling functions are plotted as a function of the baryon density for different values of the asymmetry parameter β.

Table 1. Saturation properties of the DBHF model and the correspondingly constructed relativistic mean-field functionals.

Model	n_{sat} [fm^{-3}]	k_{F} [fm^{-1}]	E/A [MeV]
DDRMF	0.143	1.28	−14.22
Renormalized DDRMF	0.168	1.36	−15.18
DBHF	0.181	1.39	−16.15

again the data for $\beta = 0.2$ which corresponds approximately to the asymmetry in an Au nucleus. From table 1, one can see that the saturation density is shifted to lower densities and the binding energy of the saturation point is weaker in the renormalized DDRMF theory compared to the original DBHF results. Without renormalization the deviations for the saturation density and the binding are even stronger. In fig. 8 the binding energy of the renormalized DDRMF theory is shown for neutron matter and symmetric nuclear matter. The results are in a fairly good agreement with the DBHF results and much better than the results without renormalization. Although the renormalized isovector coupling functions g_ρ^2 and g_δ^2 show a stronger β-dependence the assumption of only density-dependent couplings is still a good approximation. Extracting those coupling functions at the representative value of $\beta = 0.2$ both the symmetric and the neutron matter EoS are reproduced with fairly good accuracy. However, as can be seen from table 1, the mapping of DBHF onto the RMF functional leads generally to a shift of the saturation point towards lower densities and a slightly smaller binding energy. This feature, which is mainly due to the neglection of the intrinsic momentum dependence of the DBHF self-energy, has also been observed in previous works when a similar procedure was applied [23,24]. Although the most realistic, Bonn A leads in DBHF to a slightly too large saturation density [14,16] and therefore such a shift of the saturation point is in favor of the DDRMF functional when applied to finite nuclei.

5 Conclusion

In summary, we present calculations of isospin asymmetric nuclear matter in a relativistic DBHF framework based on projection techniques. The approximation scheme for the treatment of isospin asymmetric nuclear matter has been improved. First of all, the application of the Bonn potential —factually the Bonn-A potential has been used throughout this work— has been modified in order to distinguish between different proton and neutron masses by the evaluation of the potential matrix elements. The modification is essential in the *np* channel when in-medium matrix elements are evaluated.

Secondly, the T-matrix can be represented by a set of six linearly independent Lorentz invariants in the *np* channel. This sixth covariant has been chosen as proposed in [15]. However, in contrast to [15] we apply still the improved decomposition scheme of the T-matrix (subtracted T-matrix representation) [16,18–20] which minimizes on-shell ambiguities in the determination of the self-energy components.

It is found that the proton properties are, in particular, sensitive to the consequences of the adaption of the Bonn potential for isospin asymmetric nuclear matter and the introduction of a sixth covariant. The proton optical potential lies a bit lower and is steeper as compared to ref. [20], whereas the neutron optical potential is almost unaltered. Furthermore, the neutron effective mass remains practically unaffected, whereas the proton mass experiences a sizable reduction. The reason is that in neutron-rich matter proton properties depend much stronger on contributions from the *np* channel than neutron properties.

The main properties of isospin asymmetric nuclear matter remain, however, unchanged. The binding energy shows the expected quadratic dependence on the asymmetry parameter. Also the depth and the steepness of the neutron optical potential decreases with increasing asymmetry, whereas the depth and steepness of the proton optical potential still shows the opposite behavior. A strong density and momentum dependence can again be observed for the isovector optical potential. In addition, the isovector optical potential remains almost independent of the asymmetry parameter β. Our DBHF calculations based on projection techniques predict a mass splitting of $m^*_{\mathrm{D},n} < m^*_{\mathrm{D},p}$ in neutron-rich matter as expected. The nonrelativistic mass derived from our DBHF approach still shows the opposite behavior, which is in agreement with the results from nonrelativistic BHF calculations [26].

At present full Brueckner calculations are still too involved for systematic applications in finite nuclei. However, the density-dependent mean-field effective coupling functions, which are obtained from the Brueckner self-energy components, parameterize the correlations of the T-matrix in a handable way. Therefore, these coupling functions can be applied to finite nuclei within the framework of DDRMF theory [23]. Doing so, a "naive" parameterization of the DBHF results in terms of a density-dependent relativistic mean-field functional leads to a poor reproduction of the original EoS. The reason are contributions from Fock-terms which are not present at the mean field level and which have to be incorporated in an effective way. This leads to a renormalization procedure of the coupling functions which absorbs the contributions from the Fock terms. However, the results with renormalization are in a quite good agreement with the DBHF results. In other words, an accurate reproduction of the DBHF EoS requires a renormalization of the coupling functions.

Appendix A. Potential matrix elements

In this appendix we give the potential matrix elements for scalar, pseudovector, and vector mesons. Overall factors in front are omitted. In contrast to the normal expressions which are used in the Bonn codes [43], we release the assumption of equal nucleon masses. This means that particle one and two can have different masses which leads to additional independent matrix elements. Therefore, one has to consider eight instead of six independent partial waves or helicity matrix elements for the scattering of positive-energy states. For completeness, we present in the following the complete sets of matrix elements for the various OBE amplitudes. We follow the notation of ref. [43]. The potential expressions are presented in terms of helicity states. First, the expressions for the scalar mesons, the σ-meson and the δ-meson, are given here

$$\langle ++|V_s^J|++\rangle = C_s\langle ++|\phi_s|++\rangle\big(I_J^{(1)} + I_J^{(0)}\big), \quad \text{(A.1)}$$

$$\langle ++|V_s^J|--\rangle = C_s\langle ++|\phi_s|--\rangle\big(I_J^{(1)} - I_J^{(0)}\big), \quad \text{(A.2)}$$

$$\langle +-|V_s^J|+-\rangle = C_s\langle +-|\phi_s|+-\rangle\big(I_J^{(2)} + I_J^{(0)}\big), \quad \text{(A.3)}$$

$$\langle +-|V_s^J|-+\rangle = C_s\langle +-|\phi_s|-+\rangle\big(I_J^{(2)} - I_J^{(0)}\big), \quad \text{(A.4)}$$

$$\langle ++|V_s^J|+-\rangle = -C_s\langle ++|\phi_s|+-\rangle I_J^{(3)}, \quad \text{(A.5)}$$

$$\langle ++|V_s^J|-+\rangle = -C_s\langle ++|\phi_s|+-\rangle I_J^{(3)}, \quad \text{(A.6)}$$

$$\langle +-|V_s^j|++\rangle = -C_s\langle +-|\phi_s|++\rangle I_J^{(3)}, \quad \text{(A.7)}$$

$$\langle -+|V_s^J|++\rangle = -C_s\langle +-|\phi_s|++\rangle I_J^{(3)}, \quad \text{(A.8)}$$

where one has

$$C_s = \pi g_{NNs}^2 \quad \text{(A.9)}$$

and

$$\langle \lambda_1'\lambda_2'|\phi_s|\lambda_1\lambda_2\rangle = \left(1 - \frac{4\lambda_1'\lambda_1 p'p}{\epsilon_1'\epsilon_1}\right)\left(1 - \frac{4\lambda_2'\lambda_2 p'p}{\epsilon_2'\epsilon_2}\right) \quad \text{(A.10)}$$

with $\epsilon_i = E_i^* + m_i^*$. The integrals over the Legendre polynomials $I_J^{(0)} - I_J^{(6)}$ are those given in appendix B of [43].

Secondly, the expression for pseudovector mesons, the π-meson and the η-meson, are written as

$$\langle ++|V_{pv}^J|++\rangle = C_{pv}\langle ++|\phi_{pv}|++\rangle\big(I_J^{(1)} + I_J^{(0)}\big), \quad \text{(A.11)}$$

$$\langle ++|V_{pv}^J|--\rangle = C_{pv}\langle ++|\phi_{pv}|--\rangle\big(I_J^{(1)} - I_J^{(0)}\big), \quad \text{(A.12)}$$

$$\langle +-|V_{pv}^J|+-\rangle = C_{pv}\langle +-|\phi_{pv}|+-\rangle\big(I_J^{(2)} + I_J^{(0)}\big), \quad \text{(A.13)}$$

$$\langle +-|V_{pv}^J|-+\rangle = C_{pv}\langle +-|\phi_{pv}|-+\rangle\big(I_J^{(2)} - I_J^{(0)}\big), \quad \text{(A.14)}$$

$$\langle ++|V_{pv}^J|+-\rangle = -C_{pv}\langle ++|\phi_{pv}|+-\rangle I_J^{(3)}\,, \tag{A.15}$$
$$\langle ++|V_{pv}^J|-+\rangle = -C_{pv}\langle ++|\phi_{pv}|+-\rangle I_J^{(3)}\,, \tag{A.16}$$
$$\langle +-|V_{pv}^J|++\rangle = -C_{pv}\langle +-|\phi_{pv}|++\rangle I_J^{(3)}\,, \tag{A.17}$$
$$\langle -+|V_{pv}^J|++\rangle = -C_{pv}\langle +-|\phi_{pv}|++\rangle I_J^{(3)}\,, \tag{A.18}$$

where one has

$$C_{pv} = \pi\frac{g_{NNpv}^2}{4M^2} \tag{A.19}$$

and

$$\langle \lambda_1'\lambda_2'|\phi_{pv}|\lambda_1\lambda_2\rangle = (2\lambda_1'p' - 2\lambda_1 p)\left(1+\frac{4\lambda_1\lambda_1' pp'}{\epsilon_1\epsilon_1'}\right) \times(2\lambda_2'p' - 2\lambda_2 p)\left(1+\frac{4\lambda_2\lambda_2' pp'}{\epsilon_2\epsilon_2'}\right). \tag{A.20}$$

with scaling mass M. In eq. (A.20) the Blankenbecler-Sugar or Thomas approximation is used, *i.e.* the exchanged energy transfer between the two nucleons is restricted to zero. Therefore, the four-momentum transfer is $(p'-p)^\mu = (0, \mathbf{p}'-\mathbf{p})$. This approximation is later on also applied for the vector mesons.

Finally, the vector mesons, the ω-meson and the ρ-meson, are treated. The vector-meson exchange potential V_v consists of three terms: the vector-vector contribution V_{vv}, the tensor-tensor contribution V_{tt}, and the mixed vector-tensor contribution V_{vt}. The vector-vector part can be written as

$$\begin{aligned}\langle ++|V_{vv}^J|++\rangle &= C_{vv}\big[\langle ++|\phi_0|++\rangle\big(I_J^{(1)}+I_J^{(0)}\big)\\ &\quad+\langle ++|\phi_{\mathbf{v}}|++\rangle\big(I_J^{(1)}-3I_J^{(0)}\big)\big],\end{aligned} \tag{A.21}$$
$$\begin{aligned}\langle ++|V_{vv}^J|--\rangle &= C_{vv}\big[\langle ++|\phi_0|--\rangle\big(I_J^{(1)}-I_J^{(0)}\big)\\ &\quad+\langle ++|\phi_{\mathbf{v}}|--\rangle\big(I_J^{(1)}+3I_J^{(0)}\big)\big],\end{aligned} \tag{A.22}$$
$$\begin{aligned}\langle +-|V_{vv}^J|+-\rangle &= C_{vv}\big[\langle +-|\phi_0|+-\rangle\\ &\quad+\langle +-|\phi_{\mathbf{v}}|+-\rangle\big]\big(I_J^{(2)}+I_J^{(0)}\big),\end{aligned} \tag{A.23}$$
$$\begin{aligned}\langle +-|V_{vv}^J|-+\rangle &= C_{vv}\big[\langle +-|\phi_0|-+\rangle\\ &\quad+\langle +-|\phi_{\mathbf{v}}|-+\rangle\big]\big(I_J^{(2)}-I_J^{(0)}\big),\end{aligned} \tag{A.24}$$
$$\begin{aligned}\langle ++|V_{vv}^J|+-\rangle &= -C_{vv}\big[\langle ++|\phi_0|+-\rangle\\ &\quad+\langle ++|\phi_{\mathbf{v}}|+-\rangle\big]I_J^{(3)}\,,\end{aligned} \tag{A.25}$$
$$\begin{aligned}\langle ++|V_{vv}^J|-+\rangle &= -C_{vv}\big[\langle ++|\phi_0|+-\rangle\\ &\quad+\langle ++|\phi_{\mathbf{v}}|+-\rangle\big]I_J^{(3)}\,,\end{aligned} \tag{A.26}$$
$$\begin{aligned}\langle +-|V_{vv}^J|++\rangle &= -C_{vv}\big[\langle +-|\phi_0|++\rangle\\ &\quad+\langle +-|\phi_{\mathbf{v}}|++\rangle\big]I_J^{(3)}\,,\end{aligned} \tag{A.27}$$
$$\begin{aligned}\langle -+|V_{vv}^J|++\rangle &= -C_{vv}\big[\langle +-|\phi_0|++\rangle\\ &\quad+\langle +-|\phi_{\mathbf{v}}|++\rangle\big]I_J^{(3)}\,,\end{aligned} \tag{A.28}$$

where one has

$$C_{vv} = \pi g_{NNv}^2\,, \tag{A.29}$$
$$\langle \lambda_1'\lambda_2'|\phi_0|\lambda_1\lambda_2\rangle = \left(1+\frac{4\lambda_1'\lambda_1 p'p}{\epsilon_1'\epsilon_1}\right)\left(1+\frac{4\lambda_2'\lambda_2 p'p}{\epsilon_2'\epsilon_2}\right), \tag{A.30}$$

and

$$\langle \lambda_1'\lambda_2'|\phi_{\mathbf{v}}|\lambda_1\lambda_2\rangle = -\left(\frac{2\lambda_1'p'}{\epsilon_1'}+\frac{2\lambda_1 p}{\epsilon_1}\right)\left(\frac{2\lambda_2'p'}{\epsilon_2'}+\frac{2\lambda_2 p}{\epsilon_2}\right). \tag{A.31}$$

The tensor-tensor part is

$$\begin{aligned}\langle ++|V_{tt}^J|++\rangle &= C_{tt}\big[\langle ++|\phi_{1t}|++\rangle\big(I_J^{(1)}+I_J^{(0)}\big)\\ &\quad+\langle ++|\phi_{1\theta}|++\rangle\big(I_J^{(4)}+I_J^{(1)}\big)\\ &\quad+\langle ++|\phi_{\sigma t}|++\rangle\big(I_J^{(1)}-3I_J^{(0)}\big)\big],\end{aligned} \tag{A.32}$$
$$\begin{aligned}\langle ++|V_{tt}^J|--\rangle &= C_{tt}\big[\langle ++|\phi_{1t}|--\rangle\big(I_J^{(1)}-I_J^{(0)}\big)\\ &\quad+\langle ++|\phi_{1\theta}|--\rangle\big(I_J^{(4)}-I_J^{(1)}\big)\\ &\quad+\langle ++|\phi_{\sigma t}|--\rangle\big(I_J^{(1)}+3I_J^{(0)}\big)\big],\end{aligned} \tag{A.33}$$
$$\begin{aligned}\langle +-|V_{tt}^J|+-\rangle &= C_{tt}\big[\langle +-|\phi_{1t}|+-\rangle\\ &\quad+\langle +-|\phi_{\sigma t}|+-\rangle\big]\big(I_J^{(2)}+I_J^{(0)}\big)\\ &\quad+\langle +-|\phi_{1\theta}|+-\rangle\big(I_J^{(5)}+I_J^{(1)}\big),\end{aligned} \tag{A.34}$$
$$\begin{aligned}\langle +-|V_{tt}^J|-+\rangle &= C_{tt}\big[\langle +-|\phi_{1t}|-+\rangle\\ &\quad+\langle +-|\phi_{\sigma t}|-+\rangle\big]\big(I_J^{(2)}-I_J^{(0)}\big)\\ &\quad+\langle +-|\phi_{1\theta}|-+\rangle\big(I_J^{(5)}-I_J^{(1)}\big),\end{aligned} \tag{A.35}$$
$$\begin{aligned}\langle ++|V_{tt}^J|+-\rangle &= -C_{tt}\big[\big[\langle ++|\phi_{1t}|+-\rangle\\ &\quad+\langle ++|\phi_{\sigma t}|+-\rangle\big]I_J^{(3)}\\ &\quad+\langle ++|\phi_{1\theta}|+-\rangle I_J^{(6)}\big],\end{aligned} \tag{A.36}$$
$$\begin{aligned}\langle ++|V_{tt}^J|-+\rangle &= -C_{tt}\big[\big[\langle ++|\phi_{1t}|+-\rangle\\ &\quad+\langle ++|\phi_{\sigma t}|+-\rangle\big]I_J^{(3)}\\ &\quad+\langle ++|\phi_{1\theta}|+-\rangle I_J^{(6)}\big],\end{aligned} \tag{A.37}$$
$$\begin{aligned}\langle +-|V_{tt}^J|++\rangle &= -C_{tt}\big[\big[\langle +-|\phi_{1t}|++\rangle\\ &\quad+\langle +-|\phi_{\sigma t}|++\rangle\big]I_J^{(3)}\\ &\quad+\langle +-|\phi_{1\theta}|++\rangle I_J^{(6)}\big],\end{aligned} \tag{A.38}$$
$$\begin{aligned}\langle -+|V_{tt}^J|++\rangle &= -C_{tt}\big[\big[\langle +-|\phi_{1t}|++\rangle\\ &\quad+\langle +-|\phi_{\sigma t}|++\rangle\big]I_J^{(3)}\\ &\quad+\langle +-|\phi_{1\theta}|++\rangle I_J^{(6)}\big],\end{aligned} \tag{A.39}$$

where one uses

$$C_{tt} = \pi\frac{g_{NNt}^2}{4M^2}\,. \tag{A.40}$$

Furthermore, one has

$$\langle \lambda_1'\lambda_2'|\phi_{1\theta}|\lambda_1\lambda_2\rangle = 2pp'\left(1-\frac{4\lambda_1'\lambda_1 p'p}{\epsilon_1\epsilon_1'}\right)\left(1-\frac{4\lambda_2'\lambda_2 p'p}{\epsilon_2'\epsilon_2}\right), \tag{A.41}$$

$$\begin{aligned}\langle\lambda_1'\lambda_2'|\phi_{\sigma t}|\lambda_1\lambda_2\rangle =& -\left(\frac{2\lambda_1 p}{\epsilon_1}+\frac{2\lambda_1' p'}{\epsilon_1'}\right)\left(\frac{2\lambda_2 p}{\epsilon_2}+\frac{2\lambda_2' p'}{\epsilon_2'}\right)\\ &\times(m_1^*+m_1'^*)(m_2^*+m_2'^*)-(E_1'^*-E_1^*)(E_2'^*-E_2^*)\\ &\times\left(\frac{2\lambda_1 p}{\epsilon_1}-\frac{2\lambda_1' p'}{\epsilon_1'}\right)\left(\frac{2\lambda_2 p}{\epsilon_2}-\frac{2\lambda_2' p'}{\epsilon_2'}\right)\\ &+(m_2^*+m_2'^*)(E_1'^*-E_1^*)\\ &\times\left(\frac{2\lambda_1 p_1}{\epsilon_1}-\frac{2\lambda_1' p_1'}{\epsilon_1'}\right)\left(\frac{2\lambda_2 p_2}{\epsilon_2}+\frac{2\lambda_2' p_2'}{\epsilon_2'}\right)\\ &+(m_1^*+m_1'^*)(E_2'^*-E_2^*)\\ &\times\left(\frac{2\lambda_1 p_1}{\epsilon_1}+\frac{2\lambda_1' p_1'}{\epsilon_1'}\right)\left(\frac{2\lambda_2 p_2}{\epsilon_2}-\frac{2\lambda_2' p_2'}{\epsilon_2'}\right), \qquad \text{(A.42)}\end{aligned}$$

and

$$\begin{aligned}\langle\lambda_1'\lambda_2'|\phi_{1t}|\lambda_1\lambda_2\rangle =& A_{tt}\left(1+\frac{4\lambda_1'\lambda_1 p'p}{\epsilon_1\epsilon_1'}\right)\left(1+\frac{4\lambda_2'\lambda_2 p'p}{\epsilon_2'\epsilon_2}\right)\\ &+B_{tt}\left(1-\frac{4\lambda_1'\lambda_1 p'p}{\epsilon_1\epsilon_1'}\right)\left(1-\frac{4\lambda_2'\lambda_2 p'p}{\epsilon_2'\epsilon_2}\right)\\ &+D_{tt}\left(1+\frac{4\lambda_1'\lambda_1 p'p}{\epsilon_1\epsilon_1'}\right)\left(1-\frac{4\lambda_2'\lambda_2 p'p}{\epsilon_2'\epsilon_2}\right)\\ &+E_{tt}\left(1-\frac{4\lambda_1'\lambda_1 p'p}{\epsilon_1\epsilon_1'}\right)\left(1+\frac{4\lambda_2'\lambda_2 p'p}{\epsilon_2'\epsilon_2}\right)\\ &+(E_1'^*-E_1^*)\left(\frac{2\lambda_1 p}{\epsilon_1}-\frac{2\lambda_1' p'}{\epsilon_1'}\right)\\ &\times(2\lambda_1' p'+2\lambda_1 p)\left(1-\frac{4\lambda_2'\lambda_2 p'p}{\epsilon_2'\epsilon_2}\right)\\ &+(E_2'^*-E_2^*)\left(\frac{2\lambda_2 p}{\epsilon_2}-\frac{2\lambda_2' p'}{\epsilon_2'}\right)\\ &\times(2\lambda_2' p'+2\lambda_2 p)\left(1-\frac{4\lambda_1'\lambda_1 p'p}{\epsilon_1'\epsilon_1}\right) \qquad \text{(A.43)}\end{aligned}$$

with $A_{tt}=(m_1^*+m_1'^*)(m_2^*+m_2'^*)$, $B_{tt}=(m_1^*+m_1'^*)^2+(m_2^*+m_2'^*)^2+(E_1'^*+E_1^*)(E_2'^*+E_2^*)+p^2+p'^2$, $D_{tt}=-(E_2'^*+E_2^*+E_1^*+E_1'^*)(m_1^*+m_1'^*)$, and $E_{tt}=-(E_2'^*+E_2^*+E_1^*+E_1'^*)(m_2^*+m_2'^*)$. Furthermore, the mixed vector-tensor part is given by

$$\begin{aligned}\big\langle++|V_{vt}^J|++\big\rangle &= C_{vt}\big[\big\langle++|\phi_1|++\big\rangle\big(I_J^{(1)}+I_J^{(0)}\big)\\ &\quad+\big\langle++|\phi_\sigma|++\big\rangle\big(I_J^{(1)}-3I_J^{(0)}\big)\big], \qquad \text{(A.44)}\\ \big\langle++|V_{vt}^J|--\big\rangle &= C_{vt}\big[\big\langle++|\phi_1|--\big\rangle\big(I_J^{(1)}-I_J^{(0)}\big)\\ &\quad+\big\langle++|\phi_\sigma|--\big\rangle\big(I_J^{(1)}+3I_J^{(0)}\big)\big], \qquad \text{(A.45)}\\ \big\langle+-|V_{vt}^J|+-\big\rangle &= C_{vt}\big[\big\langle+-|\phi_1|+-\big\rangle\\ &\quad+\big\langle+-|\phi_\sigma|+-\big\rangle\big]\big(I_J^{(2)}+I_J^{(0)}\big), \qquad \text{(A.46)}\\ \big\langle+-|V_{vt}^J|-+\big\rangle &= C_{vt}\big[\big\langle+-|\phi_1|-+\big\rangle\\ &\quad+\big\langle+-|\phi_\sigma|-+\big\rangle\big]\big(I_J^{(2)}-I_J^{(0)}\big), \qquad \text{(A.47)}\\ \big\langle++|V_{vt}^J|+-\big\rangle &= -C_{vt}\big[\big\langle++|\phi_1|+-\big\rangle\\ &\quad+\big\langle++|\phi_\sigma|+-\big\rangle\big]I_J^{(3)}, \qquad \text{(A.48)}\\ \big\langle++|V_{vt}^J|-+\big\rangle &= -C_{vt}\big[\big\langle++|\phi_1|-+\big\rangle\\ &\quad+\big\langle++|\phi_\sigma|-+\big\rangle\big]I_J^{(3)}, \qquad \text{(A.49)}\\ \big\langle+-|V_{vt}^J|++\big\rangle &= -C_{vt}\big[\big\langle+-|\phi_1|++\big\rangle\\ &\quad+\big\langle+-|\phi_\sigma|++\big\rangle\big]I_J^{(3)}, \qquad \text{(A.50)}\\ \big\langle-+|V_{vt}^J|++\big\rangle &= -C_{vt}\big[\big\langle+-|\phi_1|++\big\rangle\\ &\quad+\big\langle+-|\phi_\sigma|++\big\rangle\big]I_J^{(3)}, \qquad \text{(A.51)}\end{aligned}$$

where one has

$$C_{vt}=\pi\frac{g_{NNv}g_{NNt}}{2M}, \qquad \text{(A.52)}$$

$$\langle\lambda_1'\lambda_2'|\phi_1|\lambda_1\lambda_2\rangle=\left[A_{vt}+D_{vt}\frac{16\lambda_1'\lambda_2'\lambda_1\lambda_2 p'^2p^2}{\epsilon_1'\epsilon_2'\epsilon_1\epsilon_2}\right], \qquad \text{(A.53)}$$

and

$$\begin{aligned}&\langle\lambda_1'\lambda_2'|\phi_\sigma|\lambda_1\lambda_2\rangle =\\ &(m_1^*+m_1'^*+m_2^*+m_2'^*)\langle\lambda_1'\lambda_2'|\phi_{\mathbf{v}}|\lambda_1\lambda_2\rangle\\ &+(E_1'^*-E_1^*)\left(\frac{2\lambda_1 p}{\epsilon_1}-\frac{2\lambda_1' p'}{\epsilon_1'}\right)\left(\frac{2\lambda_2 p}{\epsilon_2}+\frac{2\lambda_2' p'}{\epsilon_2'}\right)\\ &+(E_2'^*-E_2^*)\left(\frac{2\lambda_1 p}{\epsilon_1}+\frac{2\lambda_1' p'}{\epsilon_1'}\right)\left(\frac{2\lambda_2 p}{\epsilon_2}-\frac{2\lambda_2' p'}{\epsilon_2'}\right) \qquad \text{(A.54)}\end{aligned}$$

with $A_{vt}=2(m_1'^*+m_2'^*+m_1^*+m_2^*-E_1'^*-E_2'^*-E_1^*-E_2^*)$ and $D_{vt}=2(\epsilon_1'+\epsilon_2'+\epsilon_1+\epsilon_2)$. For the ω-meson only the vector-vector part contributes, because $g_{NNt}=0$ for the ω-meson.

Appendix B. Partial-wave decomposition

For a general two-body reaction with four distinct spin-1/2 particles and ignoring anti-particles, the number of independent amplitudes is sixteen. Due to parity conservation this number is reduced to eight independent amplitudes. We denote a helicity amplitude by $\langle\lambda_1'\lambda_2'|\phi^J(p',p)|\lambda_1\lambda_2\rangle$, where λ_i and λ_i' are the initial and final helicities, respectively. Therefore, we have the following set of amplitudes:

$$\begin{aligned}\phi_1^J(p',p)&=\big\langle++|\phi^J(p',p)|++\big\rangle,\\ \phi_2^J(p',p)&=\big\langle++|\phi^J(p',p)|--\big\rangle,\\ \phi_3^J(p',p)&=\big\langle+-|\phi^J(p',p)|+-\big\rangle,\\ \phi_4^J(p',p)&=\big\langle+-|\phi^J(p',p)|-+\big\rangle, \qquad \text{(B.1)}\\ \phi_5^J(p',p)&=\big\langle++|\phi^J(p',p)|+-\big\rangle,\\ \phi_6^J(p',p)&=\big\langle++|\phi^J(p',p)|-+\big\rangle,\\ \phi_7^J(p',p)&=\big\langle+-|\phi^J(p',p)|++\big\rangle,\\ \phi_8^J(p',p)&=\big\langle-+|\phi^J(p',p)|++\big\rangle.\end{aligned}$$

To partially decouple this system, it is useful to introduce the following linear combinations of helicity amplitudes:

$$\begin{aligned} T^J_{12,o} &= \phi^J_1 - \phi^J_2\,, \\ T^J_{34,o} &= \phi^J_3 - \phi^J_4\,, \\ T^J_{56,o} &= \phi^J_5 - \phi^J_6\,, \\ T^J_{78,o} &= \phi^J_7 - \phi^J_8\,, \\ T^J_{12,e} &= \phi^J_1 + \phi^J_2\,, \\ T^J_{34,e} &= \phi^J_3 + \phi^J_4\,, \\ T^J_{56,e} &= \phi^J_5 + \phi^J_6\,, \\ T^J_{78,e} &= \phi^J_7 + \phi^J_8\,. \end{aligned} \tag{B.2}$$

In solving the coupled scattering equation using the linear combinations of the helicity amplitudes, two subsets of coupled integral equations,

$$\begin{aligned} T^{12}_o &= V^{12}_o + \int V^{12}_o T^{12}_o + V^{56}_o T^{78}_o\,, \\ T^{34}_o &= V^{34}_o + \int V^{34}_o T^{34}_o + V^{78}_o T^{56}_o\,, \\ T^{56}_o &= V^{56}_o + \int V^{12}_o T^{56}_o + V^{56}_o T^{34}_o\,, \\ T^{78}_o &= V^{78}_o + \int V^{78}_o T^{12}_o + V^{34}_o T^{78}_o\,, \end{aligned} \tag{B.3}$$

and

$$\begin{aligned} T^{12}_e &= V^{12}_e + \int V^{12}_e T^{12}_e + V^{56}_e T^{78}_e\,, \\ T^{34}_e &= V^{34}_e + \int V^{34}_e T^{34}_e + V^{78}_e T^{56}_e\,, \\ T^{56}_e &= V^{56}_e + \int V^{12}_e T^{56}_e + V^{56}_e T^{34}_e\,, \\ T^{78}_e &= V^{78}_e + \int V^{78}_e T^{12}_e + V^{34}_e T^{78}_e\,, \end{aligned} \tag{B.4}$$

emerge. Equation (B.3) is a coupled spin singlet-triplet state, whereas eq. (B.4) is a coupled triplet state. For identical particles the coupled spin singlet-triplet state of eq. (B.3) decouples further into a decoupled singlet state

$$T^{12}_o = V^{12}_o + \int V^{12}_o T^{12}_o \tag{B.5}$$

and a decoupled triplet state

$$T^{34}_o = V^{34}_o + \int V^{34}_o T^{34}_o \tag{B.6}$$

due to ${}^{56}V^J_o = {}^{78}V^J_o = {}^{56}T^J_o = {}^{78}T^J_o = 0$.

References

1. H.A. Bethe, Rev. Mod. Phys. **62**, 801 (1990).
2. C.J. Pethick, D.G. Ravenhall, C.P. Lorentz, Nucl. Phys. A **584**, 675 (1995).
3. J.M. Lattimer, C.J. Pethick, M. Prakash, P. Haensel, Phys. Rev. Lett. **66**, 2701 (1991); E.N.E. van Dalen, A.E.L. Dieperink, J.A. Tjon, Phys. Rev. C **67**, 065807 (2003).
4. T. Klähn, D. Blaschke, S. Typel, E.N.E. van Dalen, A. Faessler, C. Fuchs, T. Gaitanos, H. Grigorian, A. Ho, E.E. Kolomeitsev, M.C. Miller, G. Röpke, J. Trümper, D.N. Voskresensky, F. Weber, H.H. Wolter, Phys. Rev. C **74**, 035802 (2006).
5. M. Prakash, T.L. Ainsworth, J.M. Lattimer, Phys. Rev. Lett. **61**, 2518 (1988); L. Engvik, M. Hjorth-Jensen, E. Osnes, G. Bao, E. Oestgaard, Phys. Rev. Lett. **73**, 2650 (1994).
6. X.R. Zhou, G.F. Burgio, U. Lombardo, H.-J. Schulze, W. Zuo, Phys. Rev. C **69**, 018801 (2004).
7. I. Tanihata, Prog. Part. Nucl. Phys. **35**, 505 (1995); P.G. Hansen, A.S. Jensen, B. Jonson, Annu. Rev. Nucl. Part. Sci. **45**, 591 (1995).
8. V. Baran, M. Colonna, V. Greco, M. Di Toro, Phys. Rep. **410**, 335 (2005).
9. P.-G. Reinhard, M. Bender, Lect. Notes Phys. **641**, 249 (2004).
10. P. Ring, Prog. Part. Nucl. Phys. **73**, 193 (1996); Lect. Notes Phys. **641**, 175 (2004).
11. A. Akmal, V.R. Pandharipande, D.G. Ravenhall, Phys. Rev. C **58**, 1804 (1998).
12. A. Lejeune, U. Lombardo, W. Zuo, Phys. Lett. B **477**, 45 (2000).
13. B. ter Haar, R. Malfliet, Phys. Rep. **149**, 207 (1987).
14. R. Brockmann, R. Machleidt, Phys. Rev. C **42**, 1965 (1990).
15. F. de Jong, H. Lenske, Phys. Rev. C **58**, 890 (1998).
16. T. Gross-Boelting, C. Fuchs, Amand Faessler, Nucl. Phys. A **648**, 105 (1999).
17. D. Alonso, F. Sammarruca, Phys. Rev. C **67**, 054301 (2003).
18. E.N.E. van Dalen, C. Fuchs, Amand Faessler, Nucl. Phys. A **744**, 227 (2004).
19. E.N.E. van Dalen, C. Fuchs, Amand Faessler, Phys. Rev. Lett. **95**, 022302 (2005).
20. E.N.E. van Dalen, C. Fuchs, Amand Faessler, Phys. Rev. C **72**, 065803 (2005).
21. J. Carlson, J. Morales, V.R. Pandharipande, D.G. Ravenhall, Phys. Rev. C **68**, 025802 (2003); W.H. Dickhoff, C. Barbieri, Prog. Part. Nucl. Phys. **52**, 377 (2004).
22. J. Decharge, D. Gogny, Phys. Rev. C **21**, 1568 (1980).
23. C. Fuchs, H. Lenske, H.H. Wolter, Phys. Rev. C **52**, 3043 (1995).
24. F. Hofmann, C.M. Keil, H. Lenske, Phys. Rev. C **64**, 034314 (2001).
25. I. Bombaci, U. Lombardo, Phys. Rev. C **44**, 1892 (1991).
26. T. Frick, Kh. Gad, H. Müther, P. Czerski, Phys. Rev. C **65**, 034321 (2002); W. Zuo, L.G. Cao, B.A. Li, U. Lombardo, C.W. Shen, Phys. Rev. C **72**, 014005 (2005).
27. B. Liu, V. Greco, V. Baran, M. Colonna, M. Di Toro, Phys. Rev. C **65**, 045201 (2002).
28. R. Machleidt, Adv. Nucl. Phys. **19**, 189 (1989).
29. C.J. Horowitz, B.D. Serot, Nucl. Phys. A **464**, 613 (1987).
30. L. Sehn, C. Fuchs, A. Faessler, Phys. Rev. C **56**, 216 (1997).
31. H.A. Bethe, B.H. Brandow, A.G. Petschek, Phys. Rev. **129**, 225 (1963).
32. K. Erkelenz, Phys. Rep. C **13**, 191 (1974).
33. M.I. Haftel, F. Tabakin, Nucl. Phys. A **158**, 1 (1970).

34. M. Rose, *Elementary Theory of Angular Momentum* (Wiley, New York, 1957).
35. J.A. Tjon, S.J. Wallace, Phys. Rev. C **32**, 267 (1985).
36. R.B. Wiringa, V.G.J. Stoks, R. Schiavilla, Phys. Rev. C **51**, 38 (1995).
37. B.S. Pudliner, V.R. Pandharipande, J. Carlson, R.B. Wiringa, Phys. Rev. Lett. **74**, 4396 (1995).
38. S. Gandolfi, F. Pederiva, S. Fantoni, K.E. Schmidt, nucl-th/0607022.
39. FOPI Collaboration (G. Stoicea *et al.*), Phys. Rev. Lett. **92**, 072303 (2004).
40. KaoS Collaboration (C. Sturm *et al.*), Phys. Rev. Lett. **86**, 39 (2001); C. Fuchs, A. Faessler, E. Zabrodin, Y.M. Zheng, Phys. Rev. Lett. **86**, 1974 (2001); C. Fuchs, Prog. Part. Nucl. Phys. **56**, 1 (2006).
41. D.J. Nice, E.M. Splaver, I.H. Stairs, O. Löhmer, A. Jessner, M. Kramer, J.M. Cordes, Astrophys. J. **634**, 1242 (2005).
42. B.-A. Li, Phys. Rev. C **69**, 064602 (2004).
43. R. Machleidt, Phys. Rev. C **63**, 024001 (2001).